Photonic-chip-based all-optical ultra-wideband pulse generation via XPM and birefringence in a chalcogenide waveguide

Kang Tan,[1,2] David Marpaung,[1,*] Ravi Pant,[1] Feng Gao,[1,4] Enbang Li,[1] Jian Wang,[2] Duk-Yong Choi,[3] Steve Madden,[3] Barry Luther-Davies,[3] Junqiang Sun,[2] and Benjamin J. Eggleton[1]

[1]*Centre for Ultrahigh bandwidth Devices for Optical Systems (CUDOS), Institute of Photonics and Optical Science (IPOS), School of Physics, University of Sydney, New South Wales 2006, Australia*
[2]*Wuhan National Laboratory for Optoelectronics, School of Optical and Electronic Information, Huazhong University of Science and Technology, Wuhan 430074, China*
[3]*CUDOS, Laser Physics Centre, Australian National University, Canberra, ACT 0200, Australia*
[4]*MOE Key Laboratory of Weak-Light Nonlinear Photonics, TEDA Applied Physics School and School of Physics, Nankai University, Tianjin 300457, China*
[*]*d.marpaung@physics.usyd.edu.au*

Abstract: We report a photonic-chip-based scheme for all-optical ultra-wideband (UWB) pulse generation using a novel all-optical differentiator that exploits cross-phase modulation and birefringence in an As_2S_3 chalcogenide rib waveguide. Polarity-switchable UWB monocycles and doublets were simultaneously obtained with single optical carrier operation. Moreover, transmission over 40-km fiber of the generated UWB doublets is demonstrated with good dispersion tolerance. These results indicate that the proposed approach has potential applications in multi-shape, multi-modulation and long-distance UWB-over-fiber communication systems.

©2013 Optical Society of America

OCIS codes: (060.0060) Fiber optics and optical communications; (060.5625) Radio frequency photonics; (070.1170) Analog optical signal processing; (350.4010) Microwaves; (999.9999) Ultra-wideband.

References and links

1. G. R. Aiello and G. D. Rogerson, "Ultra-wideband wireless systems," IEEE Microw. Mag. **4**(2), 36–47 (2003).
2. J. Yao, F. Zeng, and Q. Wang, "Photonic generation of ultrawideband signals," J. Lightwave Technol. **25**(11), 3219–3235 (2007).
3. S. Pan and J. Yao, "UWB-over-fiber communications: Modulation and transmission," J. Lightwave Technol. **28**(16), 2445–2455 (2010).
4. C. Wang, F. Zeng, and J. Yao, "All-Fiber ultrawideband pulse generation based on spectral shaping and dispersion-induced frequency-to-time conversion," IEEE Photon. Technol. Lett. **19**(3), 137–139 (2007).
5. Q. Wang and J. Yao, "UWB doublet generation using nonlinearly-biased electro-optic intensity modulator," Electron. Lett. **42**(22), 1304–1305 (2006).
6. S. T. Abraha, C. M. Okonkwo, E. Tangdiongga, and A. M. J. Koonen, "Power-efficient impulse radio ultrawideband pulse generator based on the linear sum of modified doublet pulses," Opt. Lett. **36**(12), 2363–2365 (2011).
7. F. Zeng and J. Yao, "Ultrawideband impulse radio signal generation using a high-speed electrooptic phase modulator and a fiber-Bragg-grating-based frequency discriminator," IEEE Photon. Technol. Lett. **18**(19), 2062–2064 (2006).
8. J. Li, K. Xu, S. Fu, J. Wu, J. Lin, M. Tang, and P. Shum, "Ultra-wideband pulse generation with flexible pulse shape and polarity control using a Sagnac-interferometer-based intensity modulator," Opt. Express **15**(26), 18156–18161 (2007).
9. E. Zhou, X. Xu, K.-S. Lui, and K. K. Y. Wong, "A power-efficient ultra-wideband pulse generator based on multiple pm-im conversions," IEEE Photon. Technol. Lett. **22**(14), 1063–1065 (2010).
10. D. Marpaung, L. Chevalier, M. Burla, and C. Roeloffzen, "Impulse radio ultrawideband pulse shaper based on a programmable photonic chip frequency discriminator," Opt. Express **19**(25), 24838–24848 (2011).
11. F. Zeng and J. Yao, "An approach to ultrawideband pulse generation and distribution over optical fiber," IEEE Photon. Technol. Lett. **18**(7), 823–825 (2006).
12. Q. Wang and J. Yao, "Switchable optical UWB monocycle and doublet generation using a reconfigurable photonic microwave delay-line filter," Opt. Express **15**(22), 14667–14672 (2007).

#180508 - $15.00 USD Received 23 Nov 2012; revised 31 Dec 2012; accepted 10 Jan 2013; published 17 Jan 2013

13. M. Bolea, J. Mora, B. Ortega, and J. Capmany, "Optical UWB pulse generator using an N tap microwave photonic filter and phase inversion adaptable to different pulse modulation formats," Opt. Express **17**(7), 5023–5032 (2009).
14. J. Wang, Q. Sun, J. Sun, and W. Zhang, "All-optical UWB pulse generation using sum-frequency generation in a PPLN waveguide," Opt. Express **17**(5), 3521–3530 (2009).
15. K. Tan, J. Shao, J. Sun, and J. Wang, "Photonic ultra-wideband pulse generation, hybrid modulation and dispersion-compensation-free transmission in multi-access communication systems," Opt. Express **20**(2), 1184–1201 (2012).
16. Y. Yue, H. Huang, L. Zhang, J. Wang, J.-Y. Yang, O. F. Yilmaz, J. S. Levy, M. Lipson, and A. E. Willner, "UWB monocycle pulse generation using two-photon absorption in a silicon waveguide," Opt. Lett. **37**(4), 551–553 (2012).
17. D. Marpaung, C. Roeloffzen, R. Heideman, A. Leinse, S. Sales, and J. Capmany, "Integrated microwave photonics," arXiv:1211.4114 (2012).
18. J. Capmany, I. Gasulla, and S. Sales, "Microwave photonics: Harnessing slow light," Nat. Photonics **5**(12), 731–733 (2011).
19. M. Mirshafiei, S. LaRochelle, and L. A. Rusch, "Optical UWB waveform generation using a micro-ring resonator," IEEE Photon. Technol. Lett. **24**(15), 1316–1318 (2012).
20. V. Ta'eed, N. J. Baker, L. Fu, K. Finsterbusch, M. R. E. Lamont, D. J. Moss, H. C. Nguyen, B. J. Eggleton, D.-Y. Choi, S. Madden, and B. Luther-Davies, "Ultrafast all-optical chalcogenide glass photonic circuits," Opt. Express **15**(15), 9205–9221 (2007).
21. B. J. Eggleton, B. Luther-Davies, and K. Richardson, "Chalcogenide photonics," Nat. Photonics **5**, 141–148 (2011).
22. B. J. Eggleton, T. D. Vo, R. Pant, J. Schr, M. D. Pelusi, D. Yong Choi, S. J. Madden, and B. Luther-Davies, "Photonic chip based ultrafast optical processing based on high nonlinearity dispersion engineered chalcogenide waveguides," Laser & Photonics Reviews **6**(1), 97–114 (2012).
23. R. Pant, C. G. Poulton, D.-Y. Choi, H. Mcfarlane, S. Hile, E. Li, L. Thevenaz, B. Luther-Davies, S. J. Madden, and B. J. Eggleton, "On-chip stimulated Brillouin scattering," Opt. Express **19**(9), 8285–8290 (2011).
24. R. Pant, A. Byrnes, C. G. Poulton, E. Li, D.-Y. Choi, S. Madden, B. Luther-Davies, and B. J. Eggleton, "Photonic-chip-based tunable slow and fast light via stimulated Brillouin scattering," Opt. Lett. **37**(5), 969–971 (2012).
25. A. Byrnes, R. Pant, E. Li, D.-Y. Choi, C. G. Poulton, S. Fan, S. Madden, B. Luther-Davies, and B. J. Eggleton, "Photonic chip based tunable and reconfigurable narrowband microwave photonic filter using stimulated Brillouin scattering," Opt. Express **20**(17), 18836–18845 (2012).
26. M. Pelusi, F. Luan, T. D. Vo, M. R. E. Lamont, S. J. Madden, D. A. Bulla, D.-Y. Choi, B. Luther-Davies, and B. J. Eggleton, "Photonic-chip-based radio-frequency spectrum analyser with terahertz bandwidth," Nat. Photonics **3**(3), 139–143 (2009).
27. M. S. Rasras, D. M. Gill, S. S. Patel, K.-Y. Tu, Y.-K. Chen, A. E. White, A. T. S. Pomerene, D. N. Carothers, M. J. Grove, D. K. Sparacin, J. Michel, M. A. Beals, and L. C. Kimerling, "Demonstration of a fourth-order polezero optical filter integrated using CMOS processes," J. Lightwave Technol. **25**(1), 87–92 (2007).
28. D. Dai and J. E. Bowers, "Novel concept for ultracompact polarization splitter-rotator based on silicon nanowires," Opt. Express **19**(11), 10940–10949 (2011).
29. M. Burla, D. Marpaung, L. Zhuang, C. Roeloffzen, M. R. Khan, A. Leinse, M. Hoekman, and R. Heideman, "On-chip CMOS compatible reconfigurable optical delay line with separate carrier tuning for microwave photonic signal processing," Opt. Express **19**(22), 21475–21484 (2011).

1. Introduction

Ultrawideband (UWB) technology has attracted great interest for its large bandwidth and high data rates under unlicensed spectrum. However, the low power spectral density dictated by the spectral mask specified by the Federal Communications Commission (FCC) limits the transmission distance of UWB signals to less than 10 m [1]. By taking advantages of low transmission loss and extremely broad bandwidth offered by optical communication systems, UWB-over-fiber (UWBoF) technology has been proposed to remove this limitation. In this approach, UWB signals are generated and distributed in the optical domain [2, 3]. Over the years, different techniques have been reported for UWB pulse generation, including spectral shaping followed by frequency-to-time mapping [4], nonlinear biasing of an electro-optic modulator [5, 6], phase-to-intensity modulation conversion [7–10], spectral filtering using microwave photonics (MWP) filters [11–13], and optical nonlinearity [14–16]. These techniques have shown good results, but most of them are based on optical fibers, which can be bulky. To reach their full potential, UWBoF systems need to adopt photonic integrated circuit (PIC) technology.

Recently, the emerging field of integrated MWP [17] where PICs are used to manipulate radiofrequency signals [18] has attracted interest for its distinct advantages in terms of size, weight, power, and cost. In this context, several photonic-chip-based solutions for UWB pulse

#180508 - $15.00 USD Received 23 Nov 2012; revised 31 Dec 2012; accepted 10 Jan 2013; published 17 Jan 2013
(C) 2013 OSA

generation have recently been presented, including silicon waveguide employing two-photon absorption [16] or ring resonators for pulse shaping [10, 19]. Although impressive results have been achieved, these approaches impose several limitations. For example, the technique reported in [16] can only synthesize simple monocycle pulses by combining positive Gaussian pulses, i.e. the normal Gaussian pulses, and negative Gaussian pulses, i.e. the pulses with inverted shape of normal Gaussian ones, at two different wavelengths, while the thermo-optical tuning employed in [10, 19] with reconfiguration time of about 1 ms makes fast data modulation impossible.

Chalcogenide (ChG) photonic chips [20–25] have recently emerged as a promising platform for implementing integrated MWP. The material possesses excellent properties such as large and ultrafast third-order optical nonlinearities, low two-photon absorption and negligible free-carrier effects [20, 21]. These properties guarantee instantaneous and pure response, ideal for all-optical nonlinear signal processing [22]. Additionally, the ChG photonic chip also exhibits large stimulated Brillouin scattering gain coefficient [23], which has recently been used for integrated MWP signal processing in the form of tunable optical delay lines [24] and a reconfigurable singe band-pass microwave filter with tunable center frequency [25].

In this work, we report a photonic-chip-based scheme for UWB pulse generation that offers a wide variety of pulse shapes and the potential for a host of modulation formats. These features are achieved by using a novel all-optical differentiator based on a chalcogenide (ChG) photonic chip. We combine the effects of cross-phase modulation (XPM) and birefringence in an As_2S_3 rib waveguide to generate polarity-inverted UWB monocycles with single optical carrier from the input Gaussian pulse train. The high Kerr-nonlinearity of ChG [21] in a chip platform enables efficient XPM in a short length of 7 cm. Furthermore, we also combine these monocycles with a proper time delay to generate polarity-switchable UWB doublets and demonstrate the transmission of these doublets over a 40-km fiber link with good dispersion tolerance. Additionally, the scheme can be extended for high-speed modulation and hybrid modulation format [15]. Consequently, the proposed approach has the potential for multi-shape, multi-modulation and dispersion-compensation-free transmission UWBoF communication systems, representing a significant advance in the field of integrated MWP.

2. Principle of operation

Figure 1 shows the schematic of the proposal. The dashed box highlights the novel all-optical differentiator, where the phase-modulated probe through on-chip XPM is differentiated at the output via on-chip birefringence and mode interference. The details are as follows.

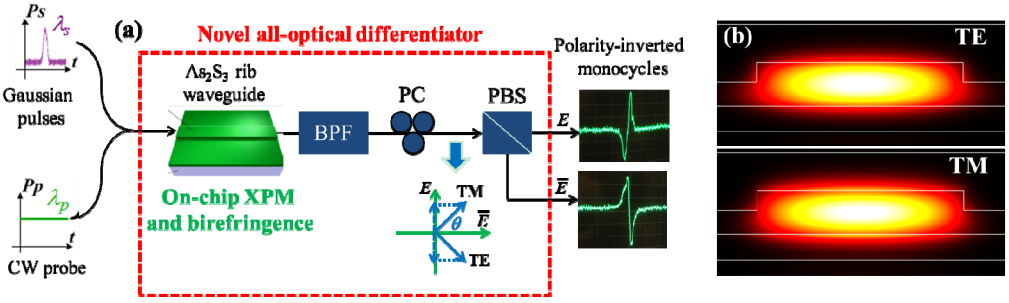

Fig. 1. (a) Schematic diagram of the proposal for photonic-chip-based UWB pulse generation. (b) TE and TM mode profiles of As_2S_3 rib waveguide.

A Gaussian optical pulse train at λ_s as pump light, $P_s(t)$, is coupled into an As_2S_3 waveguide together with a continuous-wave (CW) probe at λ_p. Due to XPM, the probe is

#180508 - $15.00 USD Received 23 Nov 2012; revised 31 Dec 2012; accepted 10 Jan 2013; published 17 Jan 2013
(C) 2013 OSA

phase modulated with a Gaussian profile, $\varphi(t)$, which is proportional to $P_s(t)$. Prior to coupling to the waveguide, the polarization of the probe light is aligned at an angle of 45°to the *x*-axis of the chip, thereby equally exciting TE and TM modes. The polarization of the signal pulses $P_s(t)$ is adjusted to compensate polarization-dependent nonlinear coefficient of these two modes such that the total phase modulation indices for both modes are the same. However, due to birefringence in the waveguide, the TE and TM modes experience a mutual time delay after 7-cm propagation. According to the simulation shown in Fig. 1(b), the two modes have different mode profiles: the TM mode has a larger optical field in the cladding and the substrate than the TE mode, and thus has a lower effective refractive index. These provide different group refractive indices for achieving the mutual time delay, τ, which is estimated to be ~12.87 ps. While in most cases the impact of on-chip birefringence is undesirable, the mutual delay between these modes is crucial to obtain the all-optical differentiation in proposed scheme.

The output from the chip is then passed to an optical band-pass filter (BPF) for removing the unwanted signal pulses. A polarization controller (PC) is then used to rotate the polarization of the probe and add a phase difference φ_0 between the TE and TM modes. Then the probe is fed into a polarization beam splitter (PBS) to achieve interference of the light at two polarizations, of which the two output ports provide signals expressed by

$$\begin{bmatrix} E(t) \\ \overline{E}(t) \end{bmatrix} \propto E_p e^{i\omega_p t} \begin{bmatrix} e^{-0.5\alpha_{TM}L + i\left[\varphi(t)+\varphi_0\right]}\cos\theta - e^{-0.5\alpha_{TE}L + i\left[\varphi(t-\tau)-\omega_p\tau\right]}\sin\theta \\ e^{-0.5\alpha_{TM}L + i\left[\varphi(t)+\varphi_0\right]}\sin\theta + e^{-0.5\alpha_{TE}L + i\left[\varphi(t-\tau)-\omega_p\tau\right]}\cos\theta \end{bmatrix}, \quad (1)$$

where α_{TE} and α_{TM} are the losses of TE and TM modes respectively, *L* is the length of ChG rib waveguide, E_p and ω_p are the electric field amplitude and optical carrier angular frequency of probe light respectively, and θ is the rotation angle compared to principal axis of PBS, as shown in the lower inset of Fig. 1(a).

When detected by photo-detector (PD), the probe at the two PBS outputs converts to photocurrents with a.c. terms expressed as

$$\begin{bmatrix} i_o(t) \\ \overline{i}_o(t) \end{bmatrix} \propto \exp\left[-0.5\left(\alpha_{TE}+\alpha_{TM}\right)L\right]\sin(2\theta) \begin{bmatrix} -\sin\left[\varphi(t)-\varphi(t-\tau)+\varphi_0+\omega_p\tau+\dfrac{\pi}{2}\right] \\ \sin\left[\varphi(t)-\varphi(t-\tau)+\varphi_0+\omega_p\tau+\dfrac{\pi}{2}\right] \end{bmatrix}. \quad (2)$$

By adjusting PC such that $\theta = \pm 45^o$ and $\varphi_0 + \omega_p\tau + \pi/2 = N\pi$ (*N* should be an integer) and considering that $\varphi(t)-\varphi(t-\tau)$ is small enough due to small τ, Eq. (2) can be simplified to

$$\begin{bmatrix} i_o(t) \\ \overline{i}_o(t) \end{bmatrix} \propto \begin{bmatrix} \mp\sin\left[\varphi(t)-\varphi(t-\tau)\right] \\ \pm\sin\left[\varphi(t)-\varphi(t-\tau)\right] \end{bmatrix} \approx \begin{bmatrix} \mp\left[\varphi(t)-\varphi(t-\tau)\right] \\ \pm\left[\varphi(t)-\varphi(t-\tau)\right] \end{bmatrix} \propto \begin{bmatrix} \mp\left[P_s(t)-P_s(t-\tau)\right] \\ \pm\left[P_s(t)-P_s(t-\tau)\right] \end{bmatrix}. \quad (3)$$

According to Eq. (3), one can conclude that, for sufficiently small τ, the output intensity from PBS can be approximated as the temporal differentiation of the phase variation of the probe, $\varphi(t)$, and hence of the input signal pulses, $P_s(t)$. Thereby, we have constructed an all-optical differentiator by exploiting XPM and birefringence in single ChG waveguide. For a Gaussian optical pulse train input, the outputs of the PBS constitute Gaussian monocycles, which are the first-order temporal derivatives of the Gaussian pulses. Note that the generated monocycles are polarity inverted, as expected from Eq. (3). At each output port, the polarity of the monocycles can be easily changed by tuning the PC to shift either *N* between odd and

#180508 - $15.00 USD Received 23 Nov 2012; revised 31 Dec 2012; accepted 10 Jan 2013; published 17 Jan 2013
(C) 2013 OSA

even or θ between 45°and –45°. Additionally, by combining the positive and negative monocycles with an appropriate time delay, polarity-inverted doublets can also be generated.

3. Experiments and discussions

Figure 2 depicts the experimental setup. The signal pulses were generated from a mode-locked laser (Calmar FPL-03CFF) at 1542.1 nm with a repetition rate of 10 MHz and pulse width around 400 fs. In order to match the FCC mask, we use dispersion compensating fiber (DCF) to broaden the pulses to a width of ~81 ps. As shown in Fig. 3(g), the broadened pulses maintained a Gaussian-like shape, to which the certain frequency chirp of generated pulses from mode-locked laser contributed. The CW probe at 1552.1 nm was from a tunable laser source (TLS, Photonetics 3642HE1570). After amplification by erbium-doped fiber amplifiers (EDFAs) and polarization adjustments, both signal and probe were injected into a 7-cm long ChG waveguide with a cross-section of 4 μm × 850 nm and a high nonlinear coefficient of ~5560 $W^{-1}\cdot km^{-1}$. The waveguide was dispersion-engineered and had a low propagation loss of less than 0.2 dB/cm [26]. The light was coupled in and out of the chip using lensed fibers. Two 99:1 couplers were placed at the input and output of the chip to monitor the chip insertion loss, which amounted to ~9 dB. The chip output was routed to a BPF for removing the pump light, which was followed by a PC and a PBS. Two 50:50 couplers were placed at the PBS outputs. For each coupler, one of the outputs was directly routed to a PD. These outputs contained two polarity-inverted monocycles and are marked as optical outputs 1 and 3 in Fig. 2.

In order to generate a doublet from these monocycles, the other outputs of the couplers were delayed using a pair of variable optical delay lines (VODLs) and combined in another 50:50 coupler. This is marked as optical output 2 in Fig. 2. To implement UWBoF transmission, the generated doublets then propagated over 40-km of single-mode fiber (SMF). The temporal waveforms and corresponding electrical spectra of the UWB pulses from each output were monitored by a digital communication analyzer (DCA, Hewlett Packard 83480A) and an electrical spectrum analyzer (ESA, Agilent E4448A), respectively.

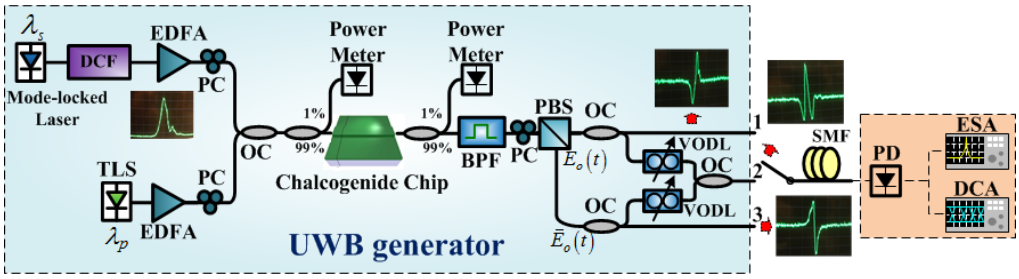

Fig. 2. The experimental setup of the proposal for photonic-chip-based UWB pulse generation with switchable pulse shape and polarity.

The measured waveforms and electrical spectra of the generated UWB pulses are shown in Figs. 3(a)-3(f). From outputs 1 and 3, polarity-inverted monocycles were generated, as shown with blue traces in Fig. 3(a) for port 1 and Fig. 3(c) for port 3. At each port, the polarity of the monocycles can easily be changed by reconfiguring the PC, as depicted with red dashed traces in Fig. 3(a) for port 1 and Fig. 3(c) for port 3. As expected, the electrical spectra of monocycles contained relatively large lower-frequency components, as shown in Figs. 3(d) and 3(f). For this reason, it is desirable to use high-order derivatives of Gaussian pulses in UWBoF systems [2], for example doublets.

The generated waveforms of polarity-switchable doublets obtained from output port 2 are shown in Fig. 3(b). As explained earlier, polarity inversion is obtained by adjusting the PC. As expected, the electrical spectra of the UWB doublets shown in Fig. 3(e) featured a higher central frequency relative to the monocycles, and thereby fitted the FCC mask (green dashed line in Fig. 3) much better than the monocycles. Moreover, the lower-frequency components

#180508 - $15.00 USD Received 23 Nov 2012; revised 31 Dec 2012; accepted 10 Jan 2013; published 17 Jan 2013
(C) 2013 OSA

can be further suppressed by exploiting well-designed antennas with a desirable frequency response curve possessing a flat top in the UWB band and a deep notch in the lower-frequency region, which performs like a band-pass filter [3].

The temporal waveform and electrical spectrum of the generated doublets after propagating through 40-km fiber without dispersion compensation are shown in Figs. 3(h) and 3(i), respectively. As evident from these figures, the doublet accumulates only a small amount of distortion in its temporal waveform and has almost the same electrical spectrum, indicating that the UWB pulses have a good tolerance to dispersion over fiber and are suitable for long-distance transmission in UWBoF communication systems. We believe that this comes from the fact that the phase of the chirped input pulse is not transferred to the UWB waveform because XPM depends only on the intensity of the input pulses. This property combined with single carrier operation proposed in this scheme leads to a better dispersion tolerance than previously reported chip-based techniques [14, 16].

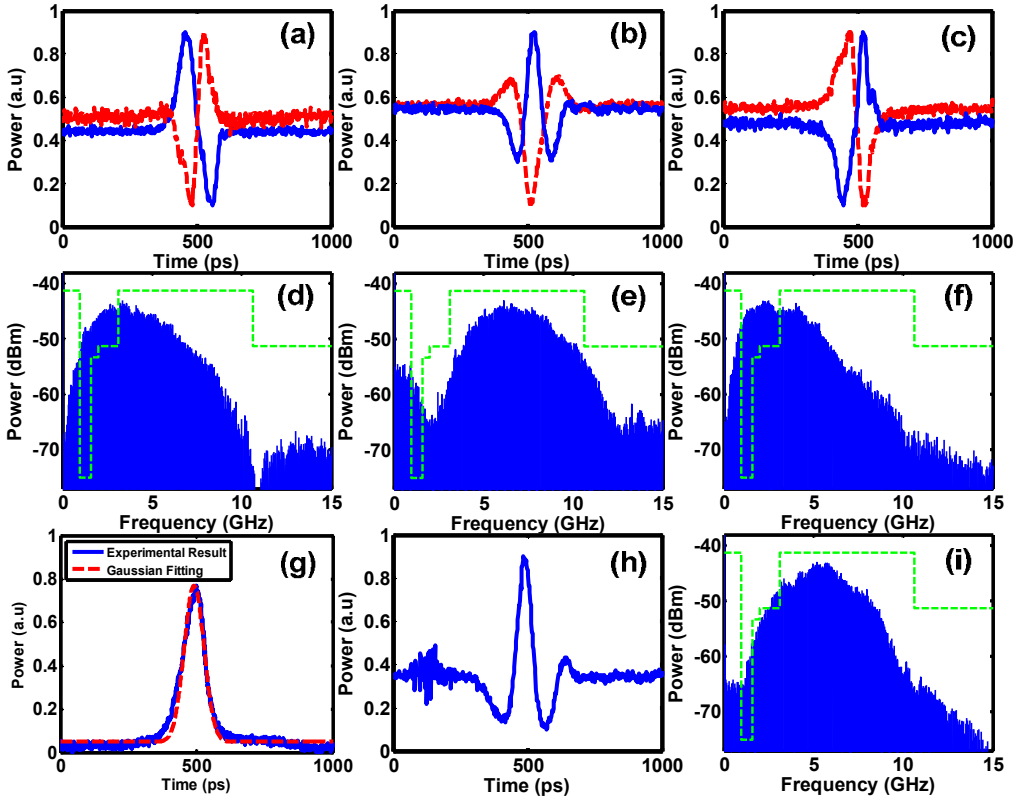

Fig. 3. (a), (b), (c) Temporal waveforms and (d), (e), (f) corresponding electrical spectra of generated UWB monocycles and doublets measured at output port 1, 2 and 3, respectively. The blue curves in (a), (b), and (c) depict the waveforms of obtained UWB pulses, while the red dashed curves show the inverted pulses after adjusting PC before PBS to shift either *N* between odd and even or θ between 45°and –45°. (g) The signal pulses measured at the output of DCF, which were then coupled with CW probe and injected into ChG chip. (h) Temporal waveforms and (i) corresponding electrical spectrum of negative doublet after propagating over 40-km SMF link. The FCC spectrum masks are added in green dashed lines.

The novelty of this scheme lies in the use of on-chip XPM and on-chip birefringence to induce a time delay between the TE and TM modes. Thus, it is useful to study the role of the on-chip time delay, τ, in the generation of the monocycle pulses. We simulated and analyzed the impact of the variation in this time delay on the properties of the output UWB pulses, as shown in Fig. 4. When the time delay changes from less than 1 ps to ~20 ps, the generated

#180508 - $15.00 USD Received 23 Nov 2012; revised 31 Dec 2012; accepted 10 Jan 2013; published 17 Jan 2013
(C) 2013 OSA

UWB pulses maintain nearly the same monocycle shape and their peak power increases almost linearly. However, when τ further increases, the pulse shape becomes slightly distorted and tends to separate into a positive Gaussian pulse followed by a negative one, as shown in the upper right inset of Fig. 4. As indicated in Fig. 4, the time delay of 12.87 ps provided by 7-cm ChG waveguide is located in the proper region for monocycle generation.

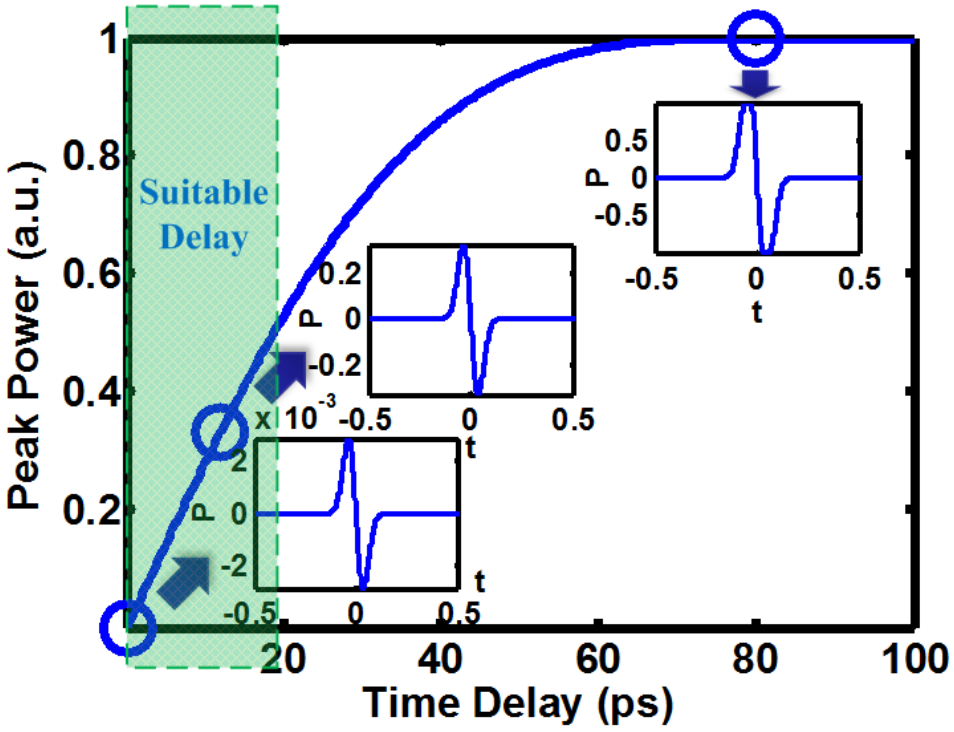

Fig. 4. Simulation results of peak power of generated monocycles as a function of mutual group time delay τ between TE and TM modes. The insets from bottom to top are the pulse shapes with τ of 0.2, 12 and 80 ps, respectively. The green block shows the proper region for monocycle generation.

4. Potential modulation techniques for multi-access UWBoF systems

For a practical UWBoF communication system, the information must be encoded, which is done by using different pulse modulation schemes such as pulse amplitude modulation (PAM), binary phase-shift keying (BPSK), pulse shape modulation (PSM), and pulse position modulation (PPM) [3]. As mentioned earlier, the proposed scheme has the advantage of flexibly implementing multi-modulation formats. In this section, we analyze the potential of implementing PAM, BPSK, PSM, PPM, and the hybrid modulation of these four [15] in the photonic-chip-based UWB generator. Note that the hybrid modulation scheme is particularly interesting to increase the transmission bit rate even further [15].

#180508 - $15.00 USD Received 23 Nov 2012; revised 31 Dec 2012; accepted 10 Jan 2013; published 17 Jan 2013
(C) 2013 OSA

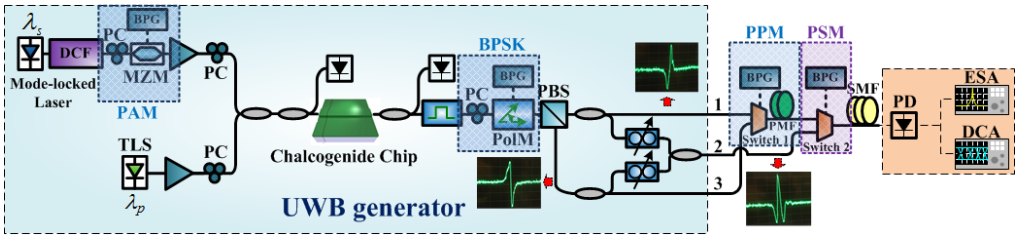

Fig. 5. Proposal for implementing PAM, BPSK, PPM, PSM and hybrid modulation format of the four into previous experimental setup

Figure 5 shows the extension of proposed scheme to accommodate multiple modulation formats. The additional hardware includes four bit-pattern generators (BPGs) for the data generation, two electro-optic modulators that include one Mach–Zehnder modulator (MZM) after the DCF and one polarization modulator (PolM) before PBS, two optical switches at the three output ports. Using this scheme, PAM can be achieved by modulating the power of the signal pulses via the MZM. Considering the cross-phase modulation index is proportional to the optical power of those signal pulses, the amplitude of the generated UWB pulses can be modified by continuously changing the driving voltage applied for MZM. In this way, the PAM with continuous tuning characteristics can be realized.

There are two methods to implement BPSK in this case. The first utilizes optical switch 1 to alternatively choose the polarity inverted UWB pulses from the PBS outputs. Alternatively one can use the PolM for either alternatively setting N as odd or even or shifting θ between 45°and −45°, according to Eq. (2). Moreover, by exploiting optical switch 2 for alternatively selecting the UWB pulse shapes between monocycle and doublet, PSM can be realized.

Finally, PPM can be achieved by using optical switch 1 to alternate UWB pulses with two orthogonal polarizations from output port 1 and 3, respectively. In this case, a length of polarization maintaining fiber (PMF) is used to provide a different group delay for the two UWB pulses at the two polarizations. By properly selecting the length of PMF, the mutual time delay between UWB pulses of two orthogonal polarizations can vary over a large range.

Thus, by exploiting the MZM for PAM, PolM for BPSK, optical switch 1 for PPM and optical switch 2 for PSM, it is possible to implement hybrid modulation of those four modulation formats to increase the transmission bit rate to at least four times the original, which is promising for future high-speed UWBoF communication [15].

In addition, the above concept can be further extended towards multi-user and multi-access UWB communication systems. Considering that all the CW probes with same proper wavelength spacing will satisfy $\varphi_0 + \omega_p \tau + \pi/2 = N\pi$ and XPM can work in a large wavelength range, polarity-switchable UWB monocycles and doublets at multi-wavelengths are potential to obtain simply by coupling more CW probes with proper wavelength spacing into the ChG chip and using wavelength-division demultiplexer to separate them at the output ports. Thus, the proposal is promising for wavelength division multiplexing (WDM) communication applied to multi-user UWB systems, where different wavelengths can be used as different channels for different users.

5. Conclusion

We have demonstrated a photonic-chip-based scheme for all-optical UWB pulse generation by exploiting on-chip XPM and on-chip birefringence in single As_2S_3 rib waveguide. By adjusting the PC and VODLs, both UWB monocycles and doublets with switchable polarity have been generated. Extension towards multi-wavelength UWB pulses with flexible pulse shape and polarity can be achieved by simply adding more CW probes with an appropriate wavelength spacing, which can be applied to multi-casting and multi-access UWB systems. The generated UWB pulses show good dispersion tolerance because the frequency chirp in the input pulses is not transferred to the output by XPM. The possibility of simultaneously implementing a number of modulation formats in this scheme has been analyzed.

#180508 - $15.00 USD Received 23 Nov 2012; revised 31 Dec 2012; accepted 10 Jan 2013; published 17 Jan 2013
(C) 2013 OSA

Finally, the scheme has the potential of on-chip and monolithic integration by integrating the discrete components like BPF [27], PBS [28], couplers and VODL [29] on a single chip. This will lead to advantages such as small size, lower loss, lighter weight and better tuning characteristics. Consequently, the proposed approach has a high potential for multi-access, multi-modulation formats and PIC-based UWBoF communication systems.

Acknowledgments

This work was funded by the Australian Research Council (ARC) through its Discovery grant (DP1096838), Federation Fellowship (FF0776056), Laureate Fellowship (FL120100029), Center of Excellence CUDOS (Grant # CE110001018), Futures Fellowship (FT110100853), the National Natural Science Foundation of China (Project number: 60977044, 61077051 and 61222502), and the Program for New Century Excellent Talents in University (NCET-11-0182). All experiments were performed at the CUDOS laboratories at the University of Sydney.

#180508 - $15.00 USD Received 23 Nov 2012; revised 31 Dec 2012; accepted 10 Jan 2013; published 17 Jan 2013
(C) 2013 OSA

213.127.10.178 {ts '2018-08-24 18:09:47'}